Structural, Optical and Electrical Properties of $Bi_{1.5}Zn_{0.92}Nb_{1.5-6x/5}W_xO_{6.92}$ Pyrochlore Ceramics

A. F. Qasrawi [a,b]* 🄰 *, Mays A. Abdalghafour[a], A. Mergen[c]*

[a]*Arab American University, Department of Physics, Jenin, Palestine*
[b]*Atilim University, Faculty of Engineering, Group of physics, 06836 Ankara, Turkey*
[c]*Marmara University, Metallurgical and Materials Engineering Department, 34722 Istanbul, Turkey*

Herein, the structural, morphological, compositional, optical, electrical and dielectric properties of $Bi_{1.5}Zn_{0.92}Nb_{1.5-6x/5}W_xO_{6.92}$ (BZN) solid solutions are reported. Tungsten substituted BZN ceramics which are fabricated by the solid state reaction technique exhibited solubility limits at substitution level below x=0.18. Remarkable engineering in the structural, optical, electrical and dielectric properties of the pyrochlore ceramics is achieved via W substitution. Namely, shrinkage in both of the lattice parameters and in the energy band gap accompanied with decrease in the microstrain, in the dielectric constant and in the electrical resistivity is observed upon increasing the W content below the solubility limit. The increase in the W content in the BZN ceramics enhances the densification of the pyrochlore and leads to higher light absorbability and larger crystallites growth. The temperature dependent electrical resistivity measurements has also shown that the pyrochlore exhibit thermal stability below 380 K.

Keywords: *$Bi_{1.5}Zn_{0.92}Nb_{1.5-6x/5}W_xO_{6.92}$, ceramics, XRD, resistivity, band gap.*

1. Introduction

The compound $Bi_{1.5}Zn_{0.92}Nb_{1.5}O_{6.92}$ (BZN) ceramics is one of the pyrochlore ceramics which finds wide range of applications[1-4]. They are regarded as low temperature cofired ceramics that is attractive for the fabrication of multiplayer devices in the high frequency and microwave ranges[1]. BZN ceramics in thin film forms are mentioned to exhibits novel electrical properties presented by high dielectric constants (~120), low loss tangent (~3×10^{-3}), extremely large breakdown voltage and energy storage density up to 98.2 mJ/cm³ [2]. The need for having microwave components with reduced size and weight without losing its properties makes the BZN pyrochlore ceramics preferable in this technology sector[3]. As practical application of these pyrochlore ceramics, hafnium doped BZN was used to fabricate varicaps. The Hf-BZN vericaps displayed series and parallel resonance exchange above 1000 MHz. When tested as microwave filters, they displayed features of microwave band-reject filter properties with notch frequencies of 1580, 1845, and 2040 MHz[4]. The importance of these filters lay in the property of being able to detect the signals of power down to 40 nW. This feature makes the BZN ceramics attractive for use in monostable - bistable circuits[4].

Owing to the above mentioned attractive features of the BZN pyrochlore ceramics, we were motivated to study the tungsten substitution effects on the BZN. The tungsten ion exhibits a lower ionic radius than that of Nb allowing atomic substations of W in sites of Nb. While Nb orbitals reach $4d^4 5s^1$, tungsten with the electronic configuration $6s^2 4f^{14} 5d^4$ can have higher orbital states forcing orbital overlapping. The

larger the orbital overlapping is, the larger the contribution of the orbital pair to the stabilization of interacting systems. The feature of less ionic radii and the atomic overlapping property which is expected to control the structural and electronic transitions in the BZN are the main reasons for selecting the tungsten as substitutional agent. Thus, the originality of this work lay in the possibility of attenuating the structural and electronic properties of the BZN by ionic substitutions. As for examples, altering the electronic band structure through imposing ions that are capable to do this issue, will lead to the narrowing of the energy band gaps making the pyrochlore ceramics more suitable for visible light sensing. The W substituted BZN pyrochlore ceramics which is synthesized by the technique of solid state reaction is characterized by the X-ray diffractometric technique, energy dispersive X-ray spectroscopy technique, scanning electron microscopy technique and optical spectrophotometry measurements. The electrical properties of the substituted ceramics are also investigated in the temperature range of 298-450 K. These techniques allow exploring the solubility limit of W in BZN, the engineering of the energy band gap, the effect of W substitution of the electrical resistivity and on the dielectric properties.

2. Experimental Details

Bismuth niobium zin oxide pyrochlore ceramics are prepared in accordance with the formula $Bi_{1.5}Zn_{0.92}Nb_{1.5-6x/5}W_xO_{6.92}$ with x being in the range of 0.1-0.30. The solid state reaction technique was employed for this purpose. In the preparation process, stoichiometric mixtures of Nb_2O_5 (99.5%, Merck), Bi_2O_3 (99.99%, Aldrich), WO_3 (99.9%, Alfa Aesar) and

*e-mail: aref.qasrawi@aaup.edu

ZnO (99.5%, Aldrich) were used. First, the powders were mixed with the help of ball (zirconia) milling technique for ~15 hours in ethanol. Then, the mixed powders were calcined at 1000 °C for 4~ hours. After that, the calcined powders were put in a agate mortar milled and then pressed into disks of 0.1 cm thicknesses and 1.0 cm diameters. As a final step, the substituted BZN pellets were sintered at 1025 °C for ~4 hours. The densities of the samples were measured by Archimedes method. The XRD diffraction technique using Miniflex 600 (CuKα radiation (λ=1.5418° A) at a scan rate of 1°/min) was used to explore the structural properties of the substituted samples. The morphology of the surfaces of the pellets were tested by a JEOL 5910LV scanning electron microscope (SEM). Using the energy dispersive X-ray spectroscopy (EDS) technique (Oxford-Inca-7274), the compositions of the samples were studied. The optical measurements were handled with the help of thermoscientific evolution 300 spectrophotometer. The dielectric constant was measured with the help of LCR meter. The temperature dependent electrical resistivity measurements was carried out using a high temperature cryostat.

3. Results and Discussion

Bismuth niobium zinc oxide pyrochlore ceramics ($Bi_{1.5}Zn_{0.92}Nb_{1.5}O_{6.92}$; BZN) is substituted in accordance with the empirical formula $Bi_{1.5}Zn_{0.92}Nb_{1.5-6x/5}W_xO_{6.92}$ (W-BZN) using the modified solid state reaction technique. The W content was altered in the region of 0.10-0.30. Figure 1a displays the X-ray diffraction (XRD) patterns for the films substituted in the x range of 0.1-0.18. The X-ray results of W substitutions above x=0.18 are not shown in Figure 1a because these samples did not show the characteristics of the single phase of BZN. In other words, above x=0.18, W is not solvable in BZN and need not to be considered. The observed XRD patterns are analyzed with using "TREOR 92" and "Cystdiff" software packages. The evaluations which targeted investigation of the structures of the studied samples allowed determining the lattice constants and the miller indices (*hkl*) for a particular structure. Many possible structural systems including cubic, hexagonal, tetragonal, trigonal, orthorhombic, monoclinic and triclinic were tested. The decisions were taken through comparing the theoretically

calculated diffraction angle (*2θ*) and related intensity with the experimentally observed ones. The maximum allowed $\Delta(2\theta) = \left|2\theta_{observed} - 2\theta_{Calculated}\right|$ difference was 0.05°. The most appropriate crystal system that suits the observed XRD patterns with least error was the cubic structure with the Miller indices that are shown in Figure 1a. The lattice parameter (*a*) for the undoped BZN samples was 10.259 *Å*. This value is comparable with that reported for BZN in literature[5,6]. The samples substituted with tungsten contents of 0.10, 0.15 and 0.18 displayed lattice parameters values of 10.131, 10.082 and 1.157 *Å*, respectively. The values are also listed in Table 1. The XRD patterns of the samples which comprises W of content of 0.18 additionally contained a peak centered at *2θ =33.85°*. This peak could not be assigned to the BZN pyrochlore ceramics but rather related to Bi_2WO_6 (JCPDS Kart No: 26-1044). The calculated weight of this phase ($W_{phase} = \Sigma \dfrac{A_{phase}}{\Sigma A_{all\ peaks}}$; *A is area under the peak*) is found to be 3.30%. It indicates that the samples have reached the solubility limits.

To get sure that the solubility limit is reached at this level of substitution, the energy dispersive X-ray spectroscopy (EDS) and scanning electron microscopy (SEM) measurements were handled. The results shown in Figure 2a and b displays an enlargement of 2000 and 5000 times for BZN comprising W of content of x=0.18, respectively. The morphology of the substituted ceramics display large grains of ~5-7 *μm* regardless of the substitution content. As also seen from Figure 2a and b, there exist another type of grains at the grain boundaries (shown by blue rectangular shape in Figure 2b). When these grains, which exist at the boundaries, were tested with the energy dispersive X-ray analyzer, they reveal the EDS spectra which are shown in Figure 2c. The atomic contents of this material were related to Bi, W and O with the correct stoichiometric formula being Bi_2WO_6. The appearance of the Zn in the spectra is mostly from the boundary regions between the BZN and Bi_2WO_6 grains. On the other hand, the EDS spectra, which were recorded from the large grains (shown by green rectangular shape in Figure 2b), displayed the spectra that are shown in Figure 2d. In contrast to what was observed in Figure 2c, this spectra indicated the unique existence of the elements composing the BZN. which are different from the ones we observed in
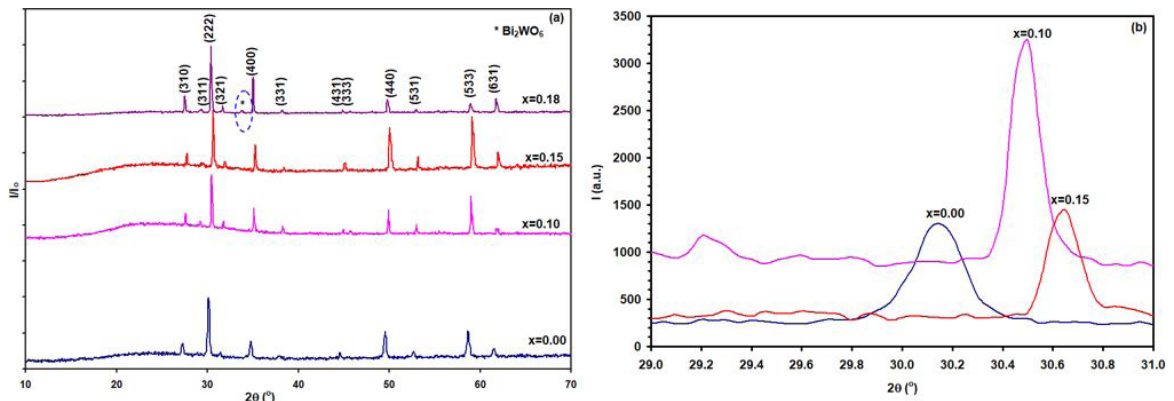

Figure 1. (a) The patterns of the X-ray diffraction and (b) the maximum peak shifts for the pure and W substituted $Bi_{1.5}Zn_{0.92}W_xNb_{1.5-6x/5}O_{6.92}$ (*0.00 ≤ x ≤ 0.18*) pyrochlore ceramics.

Figure 2c. In the light of these analyses it is possible to say that the solubility limit of tungsten in the BZN ceramics is in the range of *0.15 < x < 0.18*.

To explore the effect of W substitution on the structural parameters, the crystallite size ($D = \dfrac{0.94\lambda_{Cu\alpha}}{\beta\cos(\theta)}$; β is maximum peak broadening[7]), the microstrain ($\in = \beta/(4\tan(\theta)[7])$ and the defect concentration ($\delta = 15 \in /(aD)[7]$) were calculated and listed in Table 1. It is clear from Figure 1b that increasing the substitution content of W shifts the maximum peak position of the BZN toward larger diffraction angles. Namely, it shifts from 30.2 0° to 30.5 0° and reaches 30. 7° as the W substitution content increases from x=0.00 to x=0.10 and reaches x=0.15, respectively. The shift in the diffraction angle toward larger values indicates the shortening of the lattice parameters. In addition, as illustrated in Table 1, the observed decrease in
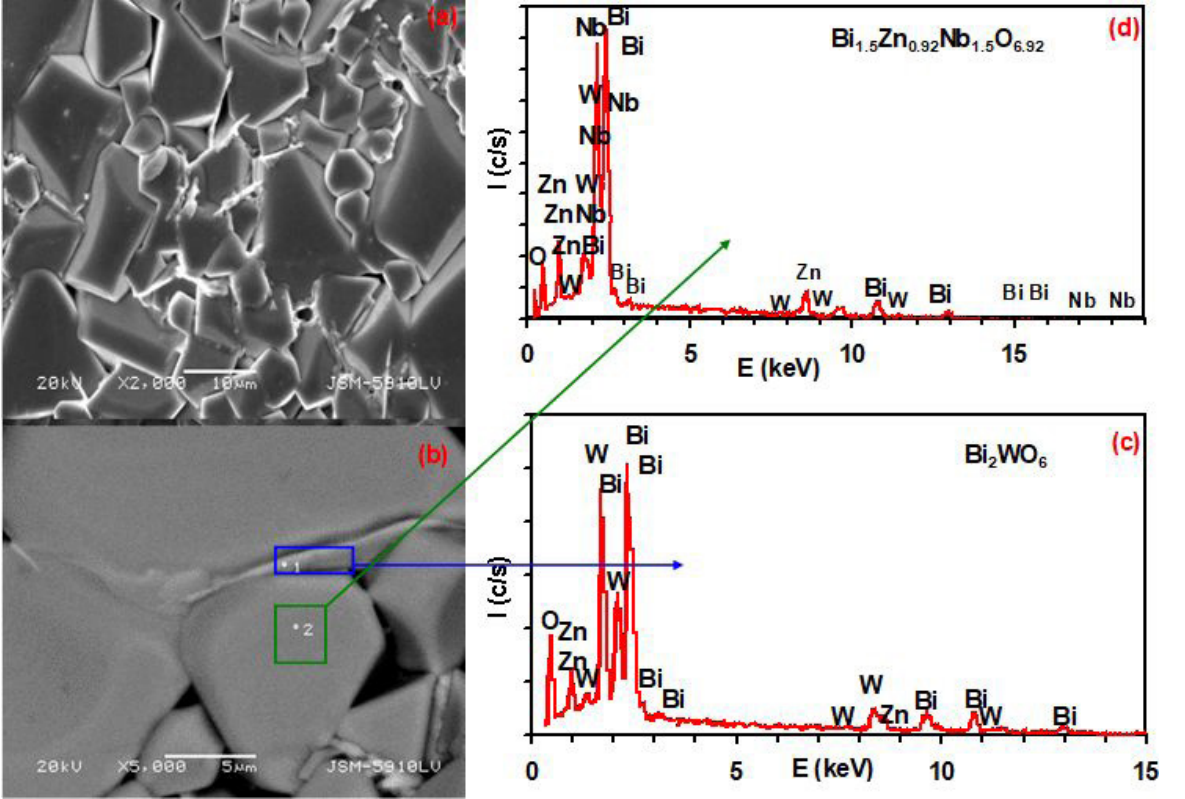
Figure 2. The scanning electron microscopy images for the $Bi_{1.5}Zn_{0.92}W_xNb_{1.5-6x/5}O_{6.92}$ (x=0.18) solid solutions. (a) an enlargement of 2000 times, (b) enlargement of 5000 times, (c) the energy dispersive X-ray spectra for point 1 shown in (b) and (d) EDS spectra for point 2 shown in (b).

Table 1. The structural, optical electrical and dielectric parameters for the W substituted $Bi_{1.5}Nb_{0.92}Zn_{1.5}O_{6.92}$ ceramics.

W content Parameter	x=0.00	x=0.10	x=0.15	x=0.18
Lattice constant a $(\mathring{A})$	10.259	10.131	10.082	10.157
Crystallite size D (nm)	34	57	57	25
Microstrain $\in (\times 10^{-3})$	3.16	2.40	2.39	5.44
Defect density $\delta\left(\times 10^{10} \; lines/cm^2\right)$	3.18	3.34	3.33	32.10
Density $\bar\rho\left(\dfrac{g}{cm^3}\right)$	6.02	6.99	7.01	7.05
Relative Density $\rho_{Relative}$ (%)	93.81	97.50	97.20	97.30
E_g (eV)	3.30*	3.85	3.40	2.65
Resistivity $\rho\left(\times 10^8 \; \Omega cm\right)$	56.30	37.63	11.86	3.16
E_ρ (eV), T>410 K	1.26	1.22	0.87	0.41
Dielectric constant (ε) @ 1.0 MHz	178	168	132	50.4

*Reported in our early works[6]

the lattice parameters is accompanied with increase in the crystallite sizes and decrease in the microstrain as well. No significant effect of the substitution is registered for the defect density (Table 1). Table 1 also shows that for the sample substituted with W of content of 0.18, the lattice parameters increases, the crystallite size decreases and both of the microstrains and defect density increases significantly. It is clear that exceeding the solubility limit by 3.3% is sufficient to alter all the structural parameters of the BZN pyrochlore ceramics. The major difference between the crystallite sizes (obtained by the X-ray diffraction technique) and grain sizes (obtained from SEM measurements) is due to the fact that the grains are composed of many crystallites. Crystallites accumulate to form grains probably due to the internal stress or defect in the structure[8,9].

The table also illustrates the effect of W substitution on the bulk density ($\bar{\rho}$) and relative density ($\rho_{Rel.} = 100.\bar{\rho} / \rho_{Theor.}$) of the BZN pyrochlore ceramics. It is clear that, the W substitution succeed in the densification of the BZN as the density and relative density increased from 6.02 g/cm^3 and from 93.81% to 6.99 g/cm^3 and to 97.50% , respectively, upon substitution with W of content of x=0.10. Further increase in the substitution content did not, remarkably, alter the bulk and relative density values. Although the lanthanum substitution with contents of 0.10, 0.20 and 0.30 revealed similar relative density values, the bulk density of the W-BZN at substitution content of x=0.10 being 6.99 g/cm^3 is higher than those of La-BZN (6.83 g/cm^3). The denser the ceramics, the higher the hardness[10].

In an attempt to explain the reasons that lay beyond the enhancement in the crystallinity and in the solidification of the BZN upon W substitution, we focus on the ionic radii of the cations and bond energies. Since the ionic radiuses of W^{+6} being 0.60 $\mathring{A}$ is less than that of Nb^{+5} (0.64 $\mathring{A}$), Bi (1.17 $\mathring{A}^5$), Zn^{+2}(0.74 $\mathring{A}^{11}$), tungsten ions can mainly occupy centers of Nb and also fills vacant sites of Bi, Zn and Nb. On the other hand, the bonding energy of Nb–O being 726 kJ/mol[12] is larger than that of W-O (661.1 kJ/mol)[13]. The higher bonding energy blocks Nb$_2$O$_5$ segregation and reduces oxygen diffusion from lattice to grain boundaries[14]. In addition, the stability of the bonded molecule is achieved with higher bond energies. The higher the bond energy is, the stronger the bond[15]. These characteristics leads to higher thermal stability and harder pyrochlore ceramics[16]. The shorter the ionic radios of W ion compared to that of Nb ions could account for the shortening of the lattice parameters and the larger crystallites that were observed upon the substitution.

Earlier studies on the formation of the Bi$_2$WO$_6$ phases in Bi$_{2-x}$La$_x$O$_6$[17] have shown that this compound is formed as a result of partial substitutions of La atoms in sites of Bi atoms in the Bi$_2$WO$_6$ structure. It is mentioned that in this process, the tungsten atom is octahedrally coordinated to oxygen atoms forming WO$_4$- layers. The Bi atom is attached to four oxygen atoms arranged in a flat tetragonal pyramid in aBi$_2$O$_2$-1ayers. The stacking of these two layers leads the formation of Bi$_2$WO$_6$ phase. In relation to our samples, with the increased content of W above x=0.15, the WO$_4$ layers start forming and self ordering with Bi$_2$O$_2$ resulting in the observed minor phase (Figure 1a).

To explore the effect of W substitution on the optical properties of the BZN powders, the pellets were carefully polished with micron polishing paper. The polishing was actualized through circulating at uniform speed for 1000 revolutions. The resulting micro powders were uniformly pressed on a crystal cleavage band to establish a uniform dense film. The band as reference was kept as base line in the spectrophotometer so that their role is subtracted and the remaining transmittance (*T*%) and reflectance (*R*%) spectra are for the W-BZN samples only. The resulting film thickness (*d*) was measured using a high sensitivity digital micrometer. The absorption coefficient ($\alpha = -ln(T / (1 - R)^2)/d^{12,16}$) spectra for the substituted W-BZN are shown in Figure 3a. In general, the shape of $\alpha - E$ variations is very similar to that we previously
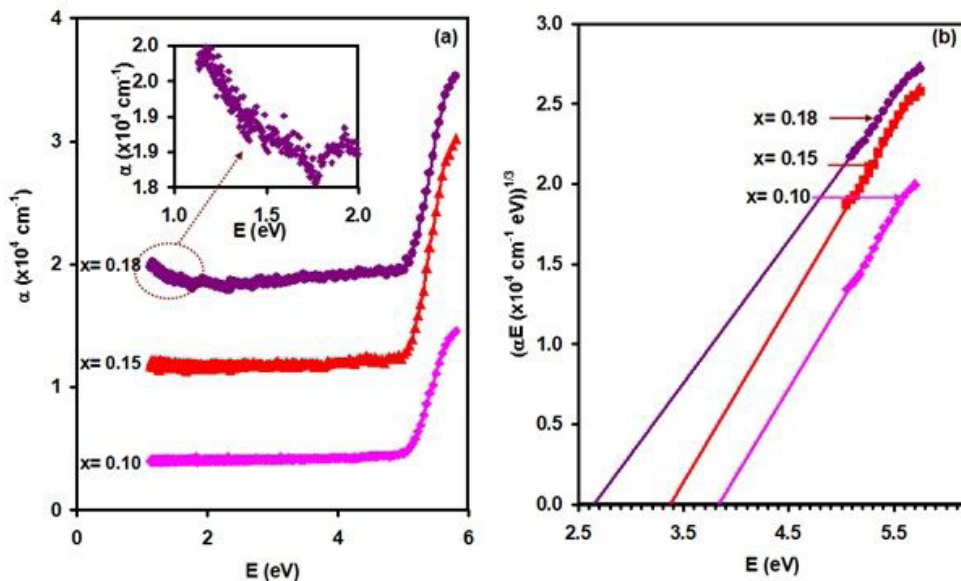
Figure 3. (a) α – spectra and (b) the Tauc's equation plotting's for the W substituted BZN ceramics.

observed for the pure BZN pyrochlore ceramics[6]. Namely, the absorption coefficient sharply decreases with decreasing incident photon energy reaching a minima near 5.0 eV where it then tends to remain constant. The absorption coefficient never reaches zero indicating the existence of interbands transitions in W-BZN. As it is seen from Figure 3a, the higher the tungsten content the higher the absorption level. As also observed from the inset of Figure 3a, the BZN samples that are substituted with W of content of x=0.18 display an increase in the values of the absorption coefficient with decreasing incident photon energy in the infrared range of light (1.75-1.14 eV). This trend of variation is an indication of the initiation of free carrier absorption mechanisms in this sample. Free carrier absorption dominates due to the lattice disturbances which can be produced by lattice vibrations, impurities and defects[18,19]. It is also believed to arise from the carrier movement affected by phonon scattering which transfers the energy to lattice when irradiated by IR light[20,21]. This belief is supported by the structural and morphological analyses which indicated the presence of Bi_2WO_6 as a minor phase in the samples containing tungsten of content of x=0.18. The minor phase increased the defects density by one order of magnitude (Table 1).

On the other hand, following our early published procedure[6,19], the energy band gap is calculated with the help of Tauc's equation[12,18,19] for indirect forbidden transitions $((\alpha E)^{1/3} = (E - E_g))$ which was the most appropriate approach that linearizes the widest range of the α spectra. The axes crossings which are illustrated in Figure 3b reveal energy band gap values of 3.85, 3.40 and 2.65 eV for BZN ceramics substituted with W of content of x=0.10, x=0.15 and x=0.18, respectively. The energy band gap decreases with increasing W content. The indirect forbidden energy band gap value of the pure BZN ceramic is 3.30 eV[6]. It is clear from the calculated values of E_g that the W substitution increased the energy band gap. It increased from 3.30 to 3.85 eV upon substitution with content of x=0.10. Many reasons may

account for the increase in the value of the energy band gap. Examples of these could be the increase in the crystallite size upon substitution[22]. Table 1 indicates that the crystallite sizes increase from 34 to 57 nm upon substitution with W of content of x=0.10. It also could be assigned to the formation of impurity levels which can move the valence band up[23]. In addition, the decrease in the energy band gap value upon increasing W content from x=0.10 to x=0.15 is assigned to the atomic orbital overlapping[24]. W with the electronic configuration $(6s^2 4f^{14} 5d^4)$ can reach higher orbital levels of BZN than Nb $(4d^4 5s^1)$. It is mentioned that the orbital overlapping of the base layer electronic states with the dopant electronic states decrease the electronic band gap through increasing the density of states values that in turn generates very dense electronic structure in substituted systems[24]. Another reason that may also account for the shrinkage in the band gap is the decrease in the lattice parameters[25]. It is mentioned that, the decrease in the value of the lattice parameters causes decreased interatomic distances which brings about reduced binding forces of the valence electrons. The reduced binding forces indicate that less energy is needed for the electrons to move from the valence to the conduction band, then reducing the E_g value[25].

The room temperature electrical resistivity (ρ) values for the pure and W substituted BZN pyrochlore ceramics with contents of x=0.00, x=0.10, x=0.15 and x=0.18 are found to be $56.30 \times 10^8 \, (\Omega cm)$, $37.63 \times 10^8 \, (\Omega cm)$, $11.86 \times 10^8 \, (\Omega cm)$ and $3.16 \times 10^8 \, (\Omega cm)$, respectively. The higher the substitution content, the lower the electrical resistivity. The decrease in the value of the electrical resistivity is assigned to the larger crystallite sizes that were achieved via increased W substitution content. Other studies which connected the effect of the crystallites sizes with the value of electrical resistivity reported the larger the crystallite sizes, the lower the electrical resistivity[26]. On the other hand, the Arrhenius plots of the resistivity are displayed in Figure 4. The plots show, approximately, temperature invariant electrical
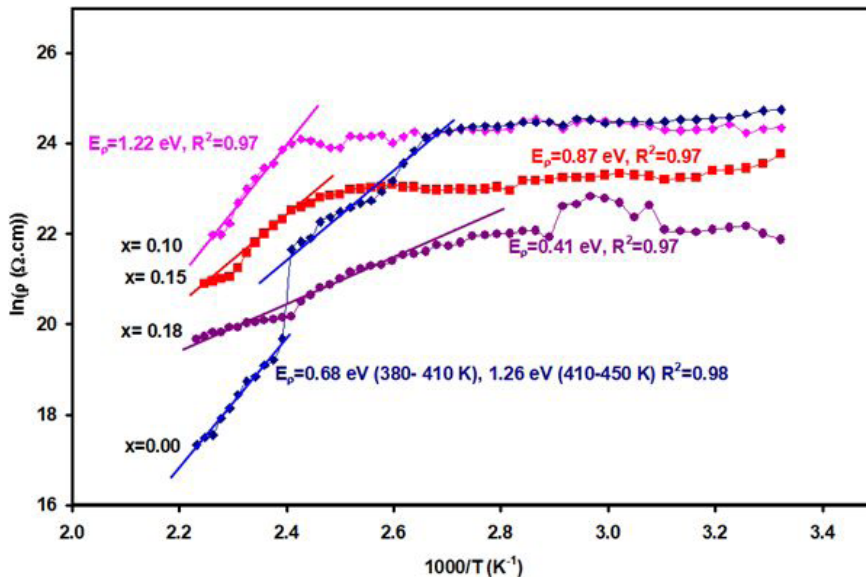
Figure 4. The temperature dependent electrical resistivity variations of W substituted BZN ceramics. The solid lines show the slopes of the Arrhenius plots.

resistivity in the temperature ranges of 298-410 K, for the samples substituted with W of content of x=0.10 and x=0.15 and in the range of 298-380 K, for the unsubstituted and samples substituted with x=0.18, respectively. In the higher temperature ranges, the electrical resistivity sharply decreases with increasing temperature following the relation, $\rho \propto exp(E_\rho / kT)$ with E_ρ being the resistivity activation energy. The calculated resistivity activation energy values which are shown in Table 1 decreased from 1.26 to 1.22, 0.87 and 0.41 eV as the W content increases from x=0.00 to x=0.10, x=0.15 and x=0.18, respectively. While the decrease in the room temperature electrical resistivity with increasing W content is assigned to the respective decrease in the energy band gaps, the decrease in the values of E_ρ indicates the extrinsic nature of conduction. The heavier the substitution, the closer the impurity levels toward the conduction band edges. This behavior could also be assigned to the more orbital overlapping that is associated with higher substitution level. Alternatively, in W-Li$_7$La$_3$Zr$_2$O$_{12}$ ceramics, the reduction in activation energy was assigned to the higher ion mobility in the grains and less resistance in W-doped grain boundaries[27]. Our XRD analyses proofed that the crystallites get larger upon substitution and this in turn reduces the crystallite boundaries[28]. The resistivity of the crystallite is much lower than that of the crystallite boundaries. The larger the crystallite size, the more pronounced the resistivity of the crystallite over that of the crystallite boundary[28].

In order to gain information about the effects of W on the dielectric properties of the BZN, the dielectric constant was measured at signal frequency of 1.0 MHz. The dielectric constant values are shown in Table 1. It is clear that the dielectric constant decreases with increasing W substitution level. Namely, it decreased from 178 to 168, 132 and 50.4 as the tungsten content increases from x=0.00 to x=0.10, x=0.15 and x=0.18, respectively. The dielectric constant decreases with increasing substitution content due to the formation of conductive networks in the substituted samples as we observed in the resistivity analyses part[29]. The same behavior which was observed for Sm substituted BZN was attributed to the mechanisms in the electronic polarizations[30]. On the other hand, at 1.0 MHz, the measured dielectric tangent loss varied in the range of 9.0×10^{-4}-2.4×10^{-3} depending on the tungsten content in the samples. The dielectric tangent loss is observed to systematically increase with increasing W content in the BZN ceramics.

In connection with the recent developments in communication sectors including 5G technology, the dielectric properties of the W-BZN need to be tested in the range of 28-39 GHz to realize its suitability for this kind of applications. Because our laboratories lack of the testing instruments in this frequency domain, we are not able to nominate the W-BZN ceramics as promising candidates for this kind technological application. Therefore, we advise interested scientists who have these testing faculties to explore the applicability of W-BZN ceramics in 5G technology. However, due to the high value and low tangent loss which indicate high quality of the W-BZN dielectric resonators, they are still attractive for storage of electromagnetic energy in the radiowave and microwave frequency domains.

4. Conclusions

In this article, we have considered the tungsten substitution effects on the Bi$_{1.5}$Zn$_{0.92}$Nb$_{1.5}$O$_{6.92}$ pyrochlore ceramics which are prepared by the solid state reaction technique. The W substitution into sites of Nb is observed to enhance the structural properties, increases the optical absorbability and engineers the energy band gap of the BZN. The decrease in the value of the energy band gap from the ultraviolet level (3.85 eV) to the visible range of light (2.65 eV) is the most significant achievement of this study. In addition, although it improves the BZN solidification through enhancing the bulk density of the BZN, the tungsten substitution decreased both the electrical resistivity and dielectric constants values. The temperature dependent electrical resistivity measurements has shown that the ceramics can exhibit stable electrical properties with temperature invariant resistivity values up to ~380 K. The resistivity activation energies which were evaluated above 410 K shifted closer to the conduction band upon increasing the substitution content of the W in the BZN.

5. Acknowledgments

6. References

1. Luo W, Li L, Guo Q, Lv X. Crystal structure and dielectric properties of Mn-substituted Bi $_{1.5}$Zn$_{1.0}$Nb$_{1.5}$O$_7$ pyrochlore ceramics as temperature stable LTCC material. J Mater Sci Mater Electron. 2017;28:5623-7.

2. Wei K, Dong H, Tan Q, Kang W, Yu S, Xiong J. Effect of precursor pH value on the structure and electrical properties of Bi1, 5Zn1, 0Nb1, 5O7 thin films. Ceram Int. 2020;46:8700-5.

3. Shihua D, Tianxiu S, Qian Z, Long H, Xiaoyun Z. Structure and dielectric properties of Ru doped Bi1, 5ZnNb1, 5O7 ceramics. Ceram Int. 2018;44:S58-60.

4. Khusayfan NM, Khanfar HK. Properties of Hf-Doped Bi 1,5 Zn 0,92 Nb 1,5 O 6,92 Ceramic Varicaps. IEEE Trans Electron Dev. 2015;63:471-5.

5. Qasrawi AF, Kmail RR, Mergen A, Genc S. Mechanical and electrical properties of Bi 1,5-x La x Zn 0,92 Nb 1,5 O 6,92 pyrochlore ceramics. J Electroceram. 2016;37:8-14.

6. Qasrawi AF, Mergen A. Energy band gap and dispersive optical parameters in Bi1, 5Zn0, 92Nb1, 5O6, 92 pyrochlore ceramics. J Alloys Compd. 2010;496:87-90.

7. Motevalizadeh L, Heidary Z, Abrishami ME. Facile template-free hydrothermal synthesis and microstrain measurement of ZnO nanorods. Bull Mater Sci. 2014;37:397-405.

8. Goktas A, Aslan F, Mutlu IH. Annealing effect on the characteristics of La 067 Sr 033 MnO 3 polycrystalline thin films produced by the sol–gel dip-coating process. J Mater Sci Mater Electron. 2012;23:605-11.

9. Goktas A, Mutlu IH, Kawashi A. Growth and characterization of La1− xAxMnO3 (A= Ag and K, x= 033) epitaxial and polycrystalline manganite thin films derived by sol–gel dip-coating technique. Thin Solid Films. 2012;520:6138-44.

10. Liu T, Chen W, Ju H, Yan S, Ma W. Characterization of YSZ Ceramic Nanopowders Synthesized at Different Temperatures

via Polyacrylamide Gel Method. J. Wuh. Univ. Technol.-. Mater. Sci. Ed. 2020;35:528-34.

11. Lai D, Yao Z, You W, Gao B, Guo Q, Lu P, et al. Modulating the energy storage performance of NaNbO3-based lead-free ceramics for pulsed power capacitors. Ceram Int. 2020;46:13511-6.

12. Marshall CP, Scholz G, Braun T, Kemnitz E. Nb-doped variants of high surface aluminium fluoride: a very strong bi-acidic solid catalyst. Dalton Trans. 2019;48:6834-45.

13. Liu W, Di J, Xue L, Li H, Oya Y, Yan Y. Phase evolution progress and properties of W-Si composites prepared by spark plasma sintering. J Alloys Compd. 2018;766:739-47.

14. Yeh TH, Hsu WC, Chou CC. Mechanical and electrical properties of ZrO (3Y) doped with RENbO (RE = Yb, Er, Y, Dy, YNd, Sm, Nd). *J. de Phys. IV Proc.* 2005;128:213-9.

15. Wang C, Xue Y, Yousaf L, Hu J, Shen Q. Effects of high hydrostatic pressure on the ordered structure including double helices and V-type single helices of rice starch. Int J Biol Macromol. 2020;144:1034-42.

16. Lu T, Liang G, Guo Z. Preparation and characterization of organic–inorganic hybrid composites based on multiepoxy silsesquioxane and cyanate resin. J Appl Polym Sci. 2006;101:3652-8.

17. Inoue Z, Watanabe A. X-ray crystallographic data on the compound Bi 2− x La x WO 6. J Mater Sci. 1980;15:2669-73.

18. Pankove Jacques I. Optical processes in semiconductors. New Jersey: Courier Corporation; 1975.

19. Skaistys E, Sugakov VI. The free-carrier absorption in polycrystals. Phys Stat Solidi. 1971;48(2):K99-101.

20. Zhang J, Wang L, Min J, Qin K, Huang J, Tang K, et al. Annealing of indium-doped CdMnTe single crystals under Cd vapors. J Cryst Growth. 2012;358:12-5.

21. Qasrawi AF, Zyoud HM. Dielectric dispersion at the Mn/ZnPc interfaces. Phys. Stat. Solidi. 2020;257:2000089.

22. Zhou H, Zeng D, Pan S. Effect of Al-induced crystallization on CdZnTe thin films deposited by radio frequency magnetron sputtering. Nucl. Inst. Meth. Phys. Res. Sec. A: Accelerators Spectrometers Detectors and Associated Equipment. 2013;698:81-3.

23. Ma Z, Ren F, Deng Y, Volinsky AA. Structural electrochemical and optical properties of Ni doped ZnO: experimental and theoretical investigation. Optik (Stuttg). 2020;219:165204.

24. Hoat DM, Naseri M, Ponce-Pérez R, Hieu NN, Vu TV, Rivas-Silva JF, et al. Reducing the electronic band gap of BN monolayer by coexistence of P (As)-doping and external electric field. Superlatt. and Microstr. 2020;137:106357.

25. Goktas A, Tumbul A, Aslan F. A new approach to growth of chemically depositable different ZnS nanostructures. J Sol-Gel Sci Technol. 2019;90:487-97.

26. Göktaş A, Tumbul A, Aslan F. Grain size-induced structural, magnetic and magnetoresistance properties of Nd 0.67 Ca 0.33 MnO 3 nanocrystalline thin films. J Sol-Gel Sci Technol. 2016;78:262-9.

27. Li Y, Wang Z, Cao Y, Du F, Chen C, Cui Z, et al. W-doped Li7La3Zr2O12 ceramic electrolytes for solid state Li-ion batteries. Electrochim Acta. 2015;180:37-42.

28. Qasrawi AF, Kayed TS, Ercan F. Heat treatment effects on the structural and electrical properties of thermally deposited AgIn5S8 thin films. Solid State Commun. 2011;151:615-8.

29. Wang G, Deng Y, Xiang Y, Guo L. Fabrication of radial ZnO nanowire clusters and radial ZnO/PVDF composites with enhanced dielectric properties. Adv Funct Mater. 2008;18:2584-92.

30. Qasrawi AF, Mergen A. Dielectric dispersion and energy band gap of Bi1, 5− xSmxZn0, 92Nb1, 5O6, 92 solid solution. Physica B. 2014;440:48-52.